PAPER

Check for updates

Roles of reaction kinetics of CO_2 on a $PrBaCo_2O_{5.5+\delta}$ surfaces†

Xing Xu,[a] Brennan Mace,[a] Erik Enriquez,[a] Shanyong Bao,[a] Zach Harrell,[a] Chonglin Chen [ID] *[a] and Myung-Hwan Whangbo[b]

A symmetric PBCO/YSZ/PBCO cell (where PBCO refers to $PrBaCo_2O_{5.5+\delta}$, and YSZ to yttria stabilized zirconia) was designed and fabricated for the investigation of the catalytic nature and reaction kinetics of CO_2 on PBCO surfaces. The electrochemical impedance spectroscopy was employed to probe the CO_2 reaction behavior on the PBCO electrode. The symmetric equivalent circuit cell characterization reveals that the surface resistance of CO_2 on PBCO is only 30.2 Ω cm^2 and the maximum surface exchange coefficient k_{chem} is 2.0×10^{-4} cm s^{-1} at 1147 K, suggesting that PBCO can be an excellent candidate for CO_2 reduction.

Introduction

Carbon dioxide (CO_2) is a stable chemical species because of its strong C=O bonds.[1] Various technologies for CO_2 reduction have been developed.[2] In the electrolysis process, CO_2 can be converted to CO or methane at the cell cathode.[3] The cathodes are normally made up of metals such as nickel,[4] platinum,[5] palladium.[6] Nickel and copper have been widely studied, but the poisonous oxidation at high CO_2 concentration shortens their catalytic life. The noble metals (Pt and Pd)[7,8] can have better chemical stability but suffer from carbon deposition on the surface, which significantly degrades their catalytic functionality. Promising catalysts for the CO_2 reduction are complex oxides because they are efficient, inexpensive and stable. Gadolinium-doped ceria (GDC) was proposed for this application,[9] and Cu-doped GDC[10] showed that its operation temperature is reduced to as low as 1023 K. However, the chemical stability of GDC-based cathode materials becomes a critical issue under reduction environment. Recently, it was demonstrated[11] that the (La, Sr)(Cr, Mn)O_3/GDC is a stable CO_2 reduction cathode for electrolyzer, and that the CO_2 reduction can be achieved by (La, Sr)TiO_3 (LSTO) and doped LSTO.[12–14] These oxides avoid the carbon deposition, but their ionic conductivity is poor so that their use requires the device to operate at high operation temperature. The Cu-doped $La_{0.58}Sr_{0.4}Co_{0.2}$-$Fe_{0.8}O_{3-\delta}$/GDC cathode can be operated at 1073–1173 K,[15] suggesting that this family of materials can be a new cathode material with good chemical stability and low operation temperature for the CO_2 reduction. Therefore, it is important to understand the kinetics of CO_2 reduction on the surface of this new class of cathode materials.

The family of $LnBaCo_2O_{5.5+\delta}$ (LnBCO) (Ln = rare earth element) has been studied as cathode materials for efficient intermediate-temperature solid oxide fuel cells (SOFCs),[16] because they have excellent transport properties,[17] low polarization resistance and low activation energy.[18,19] Especially, the ordered double perovskite $PrBaCo_2O_{5.5+\delta}$ (PBCO) exhibits superfast ionic conductivity, rapid oxygen ion diffusion and surface exchange kinetics.[20] Recently, various single crystalline thin films of LnBCO, which have highly ordered oxygen vacancies, have been fabricated for systematic studies on their physical properties and reaction kinetics.[21–23] These studies indicate that the diffusion of oxygen and hydrogen is ultrafast and occurs *via* layer-by-layer exchange diffusion with oxygen vacancies.[21] From the electrochemical impedance spectroscopy study on the symmetric cell based on the PBCO thin film electrode,[24] this electrode was found to have low polarization resistance and low activation energy than many other complex oxide systems. Thus PBCO is a prominent candidate for the low/intermediate temperature SOFC cathode material, suggesting that it would also be good for the CO_2 reduction. In this work we examine the surface chemical kinetics of CO_2 reduction on the PBCO surfaces by employing electrochemical impedance spectroscopy (EIS), with an objective to evaluate the feasibility of PBCO as the cathode material for CO_2 reduction. Our work complements the previous studies on Pt electrodes[25] and the symmetric cell GDC electrodes for the reduction of CO_2 (ref. 9) and many other materials.[26,27] In what follows we report results of our study.

[a]Department of Physics & Astronomy, The University of Texas at San Antonio, TX, 78249, USA. E-mail: cl.chen@utsa.edu

[b]Department of Chemistry, North Carolina State University, Raleigh, NC 27695-8204, USA

Experimental

The symmetric cell of PBCO/YSZ/PBCO was fabricated by pulsed laser deposition (PLD) technique. The thin films of ordered

double perovskite structure PBCO were deposited on the surfaces of the double-side polished YSZ (100) substrate. The symmetric electrodes are constrained in a round shape with 0.1 cm^2 area by Pt mask. Epitaxial PBCO thin film electrodes were grown in 250 m Torr oxygen ambient at 1123 K under the KrF Excimer laser with 248 nm wavelength, which was operated with the energy density of 1.5 J cm^{-2} and repetition rate of 5 Hz. After the deposition, the films were annealed in 200 Torr oxygen ambient at 1123 K for 15 min and cooled down by the rate of 5 K min^{-1} to room temperature. The typical thickness of as-synthesized symmetric cell electrodes is around 350 nm and the YSZ electrolyte is 0.5 mm thick and 5 mm in diameter. Details of the epitaxial growth of LnBCO thin films on various substrates were described in the previous reports.[15,18,24,28]

An as-fabricated symmetric cell was connected with platinum wires using silver paste on both electrodes of the symmetric cell. The cell was placed in the exhaust water-sealed tube furnace, and the CO_2 (99.999% pure Praxair) flow was introduced into the furnace in the flow rate of 100 cm^3 min^{-1}. The Solartron 1287/1260 system is applied to conduct the temperature dependent two-probe EIS measurement. The furnace temperature was set at a rate of 5 K min^{-1} for each temperature change and the EIS measurement was conducted at each 25 K step from 973 K to 1173 K after the temperature became stable. A constant AC amplitude of 10 mV is applied and the frequency is scanned from 1 MHz to 0.01 Hz. Three cycles of EIS measurements were carried out for the sample from 973 K to 1173 K.

Results and discussions

The microstructure of the as-grown symmetric cell is characterized by X-ray diffraction (XRD) and SEM. Fig. 1(a) shows the XRD θ–2θ spectrum of the symmetric PBCO/YSZ/PBCO cell. Only the (00l) peaks of the YSZ substrate and PBCO thin film electrode appear in the diffraction pattern, suggesting that the thin film electrode is c-axis oriented with good crystallinity (c(PBCO) = 0.763 nm and a(YSZ) = 0.5123 nm). The c-lattice parameter of PBCO thin film is equal to that of the bulk state.[29] To confirm the epitaxial quality, a tilted θ–2θ (κ rotation) was performed, as seen in Fig. 1(b), showing the 45° tilted XRD θ–2θ pattern. Only PBCO (012) and (024) appear in the pattern, confirming that the PBCO film has good single crystallinity. Fig. 1(c) is a phi-scan pattern from the (022) YSZ or (012) PBCO plane, indicating that the cubic-on-cubic growth of PBCO (001) on YSZ (001) is achieved by 45° rotation along (00l) axis to reduce the lattice misfit from 31% to 7% (Fig. 1(b) inset). It is interesting to note that the phi-scan of PBCO (012) shows a group of peaks separated in 30° each other appeared in the spectrum. These peaks can be attributed to the ordered oxygen vacancy structures and the as-induced lattice deformation. Details are still under investigation. The thickness of PBCO electrode is about 350 nm, which is obtained by the cross-section scanning electron microscopy (Fig. 1(d)). Fig. 2 shows the Nyquist plots of the temperature-dependent EIS measurements of the PBCO/YSZ/PBCO symmetric cell in pure CO_2 ambient. The Nyquist spectra consist of two overlapping compressed semi-circles but become clearly distinguishable at
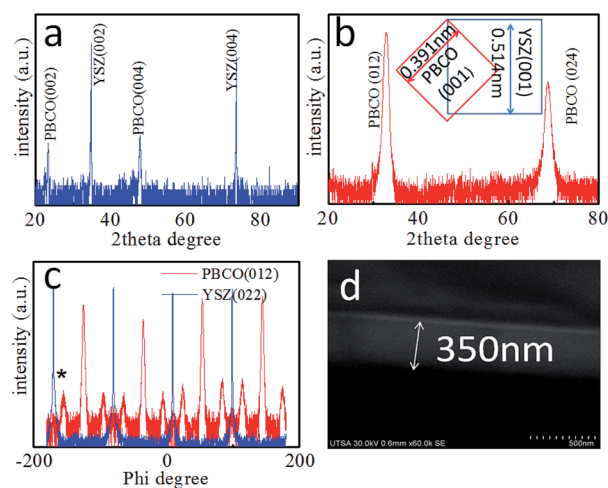

Fig. 1 (a) θ–2θ XRD profile for the PBCO/YSZ/PBCO symmetric cell. (b) The tilted θ–2θ XRD pattern of PBCO film and the inset shows the epitaxial relationship between PBCO and YSZ lattice. (c) Is the phi scan of PBCO (012): red line and YSZ (022) blue line. (d) the cross-section SEM image shows PBCO/YSZ structure. The thickness of PBCO electrode is about 350 nm.

lower temperatures. These two overlapping compressed semi-circles are attributed to electrode surface and electrode/electrolyte interface. At high temperature, the spectra reveal compressed semi-circle in which the gas–electrode interface
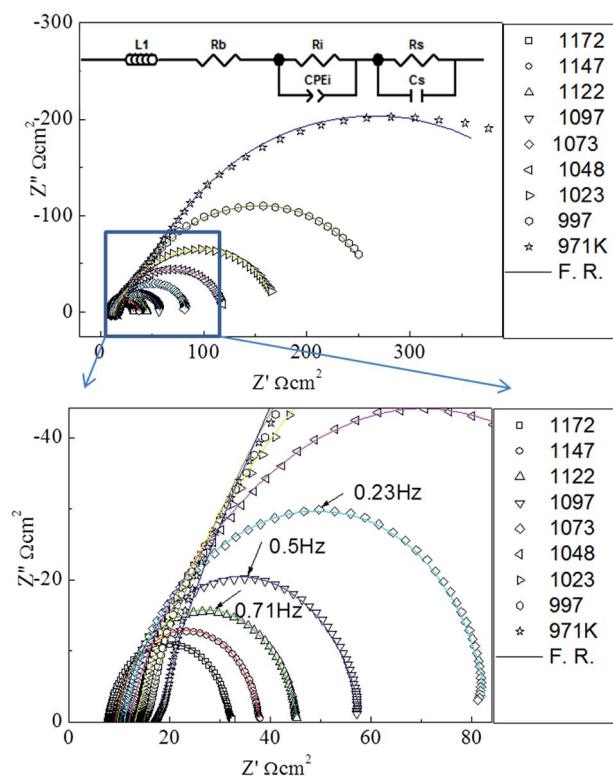

Fig. 2 The Nyquist plot of the PBCO/YSZ/PBCO symmetric cell in CO_2 ambient from 973 to 1173 K. The inset shows the equivalent circuit used for the fitting of the Nyquist plot. The solid lines are the fitting results.

contributes at low frequency region with large polarization resistance, but overlaps with the electrolyte–electrode interface at intermediate frequency. The characteristic frequency with the largest negative value of Z'' is 1 Hz at 1172 K, which is much smaller than that found for PBCO in oxygen[24] indicating that the dissociation of CO_2 is much slower than that of O_2. The latter is consistent with the finding of the previous studies that the smaller oxygen partial pressure in oxygen ambient, the smaller characteristic frequency.[30,31,31,32] At frequencies higher than 7000 Hz, a purely inductive response can be observed (*i.e.*, positive imaginary impedance), which results from the loss of ohmic conductivity between the electrolyte and the leads.

The fitting analysis of the EIS spectra data was performed by using the equivalent circuit of Zview.[33] The equivalent circuit is shown in the inset of Fig. 2, where R_b is the bulk contribution of the cell, R_s is the surface resistance of the electrochemical reaction, R_i is the interface resistance between the electrode and the electrolyte, C_s is the surface capacitance of the electrode reaction, and CPE is the capacitance in the electrode–electrolyte interface diffusion. The parallel phase (R_s, C_s) represents the surface reaction of the CO_2 molecule and the PBCO electrode, and the parallel phase (R_i, CPE) the process of the oxygen ion transportation at the PBCO/YSZ interface. The electrode contacts and the platinum wires can usually cause an inductive behavior, which is denoted by the inductance L. We employ this equivalent circuit model, similar to that employed in our previous studies on the symmetric cell EIS studies,[19,24,34,35] to characterize the dominant surface and interface processes in the chemical reactions with symmetric cell thin film electrode structures. The fitting results from the EIS data (from the cycle 2) are shown in the Table 1. The small fitting errors of R_s and C_s (<5%) and R_i (<6%) suggest that the nature of the symmetric cell structures is well described by the equivalent circuit model although it leads to errors slightly greater than those from the symmetric cell in oxygen.[34,36] This is due most likely to the complicated processes of the interaction between CO_2 and PBCO electrode.
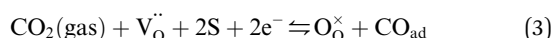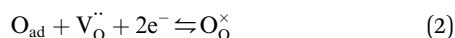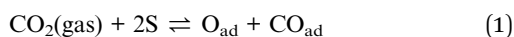
$$CO_2(gas) + 2S \rightleftharpoons O_{ad} + CO_{ad} \qquad (1)$$

$$O_{ad} + V_O^{\cdot\cdot} + 2e^- \leftrightharpoons O_O^{\times} \qquad (2)$$

$$CO_2(gas) + V_O^{\cdot\cdot} + 2S + 2e^- \leftrightharpoons O_O^{\times} + CO_{ad} \qquad (3)$$

Table 1 Parameters of the equivalent circuit extracted from the fitting analysis taken from the second-cycle EIS measurement

T, K	R_i, ohm	δR_i, error%	R_s, ohm	δR_s, error%	C_s, F	δC_s, error%
1172	81.81	3.7	241.6	1.3	0.000774	1.5
1147	91.37	3.4	302.5	1.0	0.000575	1.2
1122	105.7	3.1	432.7	0.7	0.00043	0.8
1097	141.8	3.2	629.5	0.6	0.000342	0.7
1073	223.5	3.6	899.8	0.6	0.000293	0.7
1048	400.1	4.4	1321	0.7	0.000262	0.9
1023	831.5	5.6	2045	0.91	0.000242	1.1
997	1847	6.4	3186	1.1	0.000234	1.3
971	3822	6.8	4775	1.3	0.000236	1.4

For the reduction of CO_2 on Pt/YSZ (Yttria-stabilized zirconia), it was proposed[37] that, after the dissociation of CO_2 into CO and O, the oxygen atom is adsorbed on the electrolyte surface and the CO on the Pt electrode. PBCO thin films are of the typical mixed ionic electronic conductor, so both of O and CO can be adsorbed on the PBCO electrode surfaces during the reaction of CO_2 on them. Accordingly, the dissociation reaction of CO_2 on the PBCO electrode may proceed in two steps, namely, the dissociative adsorption (eqn (1)) and the incorporation (eqn (2)) processes: where S, $V_O^{\cdot\cdot}$, and $O_O^{\times}$ denote the adsorption site, the oxygen vacancy on the PBCO surface, and the oxygen atom in the PBCO lattice, respectively. In the dissociative adsorption process, CO_2 is first adsorbed on the PBCO thin film to form various intermediates depending upon the processing temperatures.[38] At the temperature from 973 to 1173 K, the intermediates are unstable and can quickly dissociate into CO and O at the oxygen vacancy positions on the PBCO surfaces (eqn (1)). Subsequently, the adsorbed atomic O will be ionized and incorporated into the oxygen vacancy on the PBCO surface lattices (eqn (2)). The previous study[24] on the PBCO thin film electrode for the oxygen reduction showed that, at higher temperatures, the rate limiting step is not the incorporation but the adsorption process. The reactions of CO_2 and O_2 on PBCO have the same incorporation process, so that the rate limiting step in the CO_2 reduction should also be the dissociative adsorption process. This is also the reason for the much smaller characterization frequency. At 973 to 1173 K, the reaction (2) should be very fast, so that the dissociative and incorporation processes may be combined together to give eqn (3). The rate of the reaction is dominantly governed by chemisorptions or the dissociative adsorption on the limited vacancy sites on the surface.

On the PBCO electrode surface, the electrochemical reaction involves the extraction and incorporation of oxygen atom or oxygen ion. For our discussion, we assume that the charge carrier concentration is uniform inside the electrode, because the critical length of PBCO for the oxygen ion diffusion at 873 K is around 140 μm,[20] which is more than 2 orders larger than the thickness of the electrode (typically, 350 nm). The resistance of reduced PBCO is 5 orders larger than that of oxidized one.[39] Accordingly, we assume that the conductivity of the electrode is linearly proportional to the oxygen vacancy concentration, which is uniformly distributed inside the dense thin film electrodes. The rates of both the forward and backward surface reactions are taken to be unity since the processing was taken in the near equilibrium. For the reaction, a small voltage of 10 mV was applied to the symmetric cell. Then, the kinetic response of the reaction should be linear[19,24] so that the first order exchange kinetics can be written as[35,36]

$$l\frac{dc}{dt} = -k_{chem}(c - c_0) \qquad (4)$$

where l is the thickness of the electrode, c the concentration of the oxygen vacancy in the electrode, k_{chem} the constant for the surface oxygen exchange, and c_0 the initial concentration of oxygen vacancy. Since the electrical conductivity σ is linearly proportional to the concentration of the oxygen vacancy c, then

$$\exp\left(-\frac{k_{chem}t}{l}\right) = \frac{\sigma(t) - \sigma(0)}{\sigma(\infty) - \sigma(0)} = \frac{c(t) - c(0)}{c(\infty) - c(0)} \quad (5)$$

and the surface exchange constant is related to the time constant τ of the above the exponential function as

$$k_{chem} = \frac{l}{\tau} \quad (6)$$

Thus, the constant for the oxygen surface exchange process can be determined by the time constant. The frequency domain represents the process of the oxygen extraction and incorporation. Thus, the parallel of R_s and C_s circuit will determine the time constant τ.

$$\omega\tau = \omega R_s C_s = 1 \quad (7)$$

where ω is the frequency from the impedance spectra so that the chemical surface exchange coefficient can be represented by the resistance and capacitance data.

$$k_{chem} = \frac{l}{\tau} = \frac{l}{R_s C_s} \quad (8)$$

We now examine the results of our EIS measurements on the basis of the reaction kinetics discussed in the previous section. Since the dissociative adsorption and the incorporation processes of CO_2 reduction would involve some activation energies E_a, one would expect $k_{chem} \propto \exp(-E_a/RT)$. Thus, we examine the Arrhenius plots, $\ln k_{chem}$ vs. $1/T$, to probe the activation energy. In our analysis we employ the results of the second and third cycle EIS measurements, because the Arrhenius plots for the first cycle EIS measurements exhibit a nonlinear behavior unlike those of the second and third cycle data. The latter is due most likely to the fact that, during the first cycle EIS measurements, the temperature increases from 973 to 1173 K in CO_2 ambient would totally alter the oxygen vacancy distribution in the PBCO electrodes because the as-grown symmetric cells were annealed under 200 Torr oxygen at 1123 K (for further discussion, see the ESI†).

The k_{chem} of the CO_2 reduction is approximately two orders smaller than that in oxygen.[24] As presented in Fig. 3, the ln k_{chem} vs. $1/T$ plots. These are linear when T is lower than ~1073 K leading to $E_a = 1.1$ eV. The maximum of k_{chem} reaches 2.0×10^{-4} cm s^{-1} at 1147 K. As the temperature is increased above ~1073 K, the ln k_{chem} vs. $1/T$ plots become nonlinear such that E_a decreases gradually eventually becoming zero at ~1147 K and becoming negative above ~1172 K. The similar behavior of the conductivity of PBCO powder was reported by Choi.[40] To gain further insight into the change in E_a discussed above, it is important to note that k_{chem} is proportional to $1/R_s C_s$ (eqn (8)). Therefore, one should examine the Arrhenius plots, ln R_s vs. $1/T$ and ln C_s vs. $1/T$ plots. The ln $(1/R_s)$ vs. $1/T$ plot is linear in the whole temperature region (Fig. 3(a)). However, the ln$(1/C_s)$ vs. $1/T$ plot (Fig. 3(b)) is not linear for the entire measured temperature region. It is C_s that makes the ln k_{chem} vs. $1/T$ deviate from a linear behavior. By carefully examining the nonlinear behavior of the surface capacitance, it is interesting
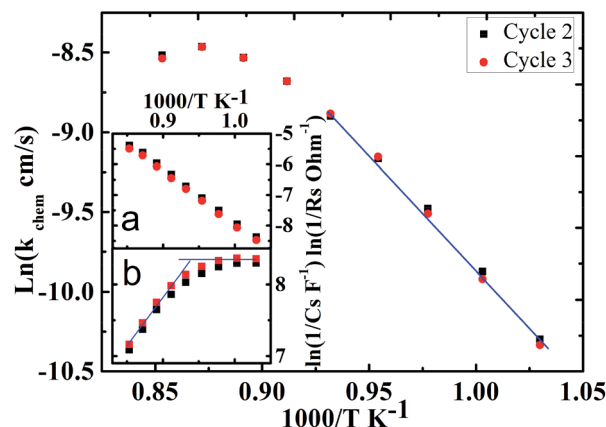

Fig. 3 The Arrhenius plots ln k_{chem} vs. $1/T$, the inset (a) ln$(1/R_s)$ vs. $1/T$, and (b) ln$(1/C_s)$ vs. $1/T$.

to find that there is a transition occurs around 1073 K in the surface capacitance curve. This transition can be interpreted to be associated with the different surface distributions in two temperature zones. (it is highly like that the order oxygen vacancy forms at the low temperature region and disorder oxygen vacancy at the high temperature region)[41] More exact to say, the surface charge density quickly changes with the increases of the temperature, which will result from the change of the oxygen vacancy structure and density at high temperatures.[42] Similar behaviors were reported in the previous research by Choi et al.[37] and the oxygen reaction kinetics in the LaBCO thin films system.[17]

Conclusions

The CO_2 reduction on the PBCO electrodes of PBCO/YSZ/PBCO symmetric cell was systematically studied by EIS measurements. The Arrhenius plot, ln k_{chem} vs. $1/T$, shows low activation energy of $E_a = 1.1$ eV below ~1073 K for the CO_2 reduction. However, the activation energy decreases gradually and becomes negative in the higher temperature region. The k_{chem} reaches a maximum 2.0×10^{-4} cm s^{-1} at 1147 K. The change in E_a at temperatures above ~1073 K can be attributed to the change in the stoichiometry of the PBCO electrode and that in the physisorption and chemisorptions mode of CO_2 on the electrode surface.

Conflicts of interest

There are no conflicts to declare.

Acknowledgements

References

1 H. J. Freund and M. W. Roberts, *Surf. Sci. Rep.*, 1996, **25**, 225–273.

2 R. J. Lim, M. S. Xie, M. A. Sk, J. M. Lee, A. Fisher, X. Wang and K. H. Lim, *Catal. Today*, 2014, **233**, 169–180.

3 M. E. Dry, *Appl. Catal., A*, 2004, **276**, 1–3.

4 T. Kim, S. Moon and S. I. Hong, *Appl. Catal., A*, 2002, **224**, 111–120.

5 G. Tao, K. R. Sridhar and C. L. Chan, *Solid State Ionics*, 2004, **175**, 615–619.

6 F. Bidrawn, G. Kim, G. Corre, J. T. S. Irvine, J. M. Vohs and R. J. Gorte, *Electrochem. Solid-State Lett.*, 2008, **11**, B167–B170.

7 G. O. Lauvstad, R. Tunold and S. Sunde, *J. Electrochem. Soc.*, 2002, **149**, E497–E505.

8 G. O. Lauvstad, R. Tunold and S. Sunde, *J. Electrochem. Soc.*, 2002, **149**, E506–E514.

9 R. D. Green, C.-C. Liu and S. B. Adler, *Solid State Ionics*, 2008, **179**, 647–660.

10 C. Y. Cheng, G. H. Kelsall and L. Kleiminger, *J. Appl. Electrochem.*, 2013, **43**, 1131–1144.

11 X. Yue and J. T. S. Irvine, *J. Electrochem. Soc.*, 2012, **159**, F442–F448.

12 O. A. Marina, N. L. Canfield and J. W. Stevenson, *Solid State Ionics*, 2002, **149**, 21–28.

13 S. Li, Y. Li, Y. Gan, K. Xie and G. Meng, *J. Power Sources*, 2012, **218**, 244–249.

14 W. Qi, Y. Gan, D. Yin, Z. Li, G. Wu, K. Xie and Y. Wu, *J. Mater. Chem. A*, 2014, **2**, 6904–6915.

15 T.-J. Huang and C.-L. Chou, *Electrochem. Commun.*, 2009, **11**, 1464–1467.

16 S. Pang, X. Jiang, X. Li, Z. Su, H. Xu, Q. Xu and C. Chen, *Int. J. Hydrogen Energy*, 2012, **37**, 6836–6843.

17 Z. Yuan, J. Liu, C. L. Chen, C. H. Wang, X. G. Luo, X. H. Chen, G. T. Kim, D. X. Huang, S. S. Wang, A. J. Jacobson and W. Donner, *Appl. Phys. Lett.*, 2007, **90**, 3.

18 J. Liu, M. Liu, G. Collins, C. Chen, X. Jiang, W. Gong, A. J. Jacobson, J. He, J. Jiang and E. I. Meletis, *Chem. Mater.*, 2010, **22**, 799–802.

19 J. Liu, G. Collins, M. Liu and C. Chen, *APL Mater.*, 2013, **1**, 031101.

20 G. Kim, S. Wang, A. J. Jacobson, L. Reimus, P. Brodersen and C. A. Mims, *J. Mater. Chem.*, 2007, **17**, 2500–2505.

21 S. Bao, C. Ma, G. Chen, X. Xu, E. Enriquez, C. Chen, Y. Zhang, J. L. Bettis Jr, M.-H. Whangbo, C. Dong and Q. Zhang, *Sci. Rep.*, 2014, **4**, 4726.

22 H. B. Wang, S. Y. Bao, J. Liu, G. Collins, C. R. Ma, M. Liu, C. L. Chen, C. Dong, M. H. Whangbo, H. M. Guo and H. J. Gao, *J. Mater. Chem. C*, 2014, **2**, 5660–5666.

23 C. Ma, M. Liu, G. Collins, J. Liu, Y. Zhang, C. Chen, J. He, J. Jiang and E. I. Meletis, *Appl. Phys. Lett.*, 2012, **101**, 021602.

24 J. Liu, G. Collins, M. Liu, C. L. Chen, J. He, J. C. Jiang and E. I. Meletis, *Appl. Phys. Lett.*, 2012, **100**, 4.

25 J. J. Sprague, O. Porat and H. L. Tuller, *Sens. Actuators, B*, 1996, **36**, 348–352.

26 S. D. Ebbesen, R. Knibbe and M. Mogensen, *J. Electrochem. Soc.*, 2012, **159**, F482–F489.

27 F. M. Sapountzi, S. Brosda, K. M. Papazisi, S. P. Balomenou and D. Tsiplakides, *J. Appl. Electrochem.*, 2012, **42**, 727–735.

28 M. Liu, J. Liu, G. Collins, C. R. Ma, C. L. Chen, J. He, J. C. Jiang, E. I. Meletis, A. J. Jacobson and Q. Y. Zhang, *Appl. Phys. Lett.*, 2010, **96**, 132106.

29 G. Kim, S. Wang, A. J. Jacobson, Z. Yuan, W. Donner, C. L. Chen, L. Reimus, P. Brodersen and C. A. Mims, *Appl. Phys. Lett.*, 2006, **88**, 024103.

30 V. C. Kournoutis, F. Tietz and S. Bebelis, *Fuel Cells*, 2009, **9**, 852–860.

31 W. Zhou, B. An, R. Ran and Z. Shao, *J. Electrochem. Soc.*, 2009, **156**, B884–B890.

32 T. Horita, K. Yamaji, N. Sakai, H. Yokokawa, A. Weber and E. Ivers-Tiffee, *Electrochim. Acta*, 2001, **46**, 1837–1845.

33 B. A. Boukamp, *Solid State Ionics*, 1986, **20**, 31–44.

34 Y. M. L. Yang, A. J. Jacobson, C. L. Chen, G. P. Luo, K. D. Ross and C. W. Chu, *Appl. Phys. Lett.*, 2001, **79**, 776–778.

35 Y. L. Yang, C. L. Chen, S. Y. Chen, C. W. Chu and A. J. Jacobson, *J. Electrochem. Soc.*, 2000, **147**, 4001–4007.

36 F. S. Baumann, J. Fleig, H. U. Habermeier and J. Maier, *Solid State Ionics*, 2006, **177**, 1071–1081.

37 J. Mizusaki, H. Tagawa, Y. Miyaki, S. Yamauchi, K. Fueki, I. Koshiro and K. Hirano, *Solid State Ionics*, 1992, **53**, 126–134.

38 U. Burghaus, *Prog. Surf. Sci.*, 2014, **89**, 161–217.

39 S. Y. Bao, X. Xu, E. Enriquez, B. E. Mace, G. Chen, S. P. Kelliher, C. L. Chen, Y. M. Zhang, M. H. Whangbo, C. Dong and Q. Y. Zhang, *Appl. Phys. Lett.*, 2015, **107**, 243903.

40 S. Choi, J. Shin and G. Kim, *J. Power Sources*, 2012, **201**, 10–17.

41 S. Streule, A. Podlesnyak, D. Sheptyakov, E. Pomjakushina, M. Stingaciu, K. Conder, M. Medarde, M. V. Patrakeev, I. A. Leonidov, V. L. Kozhevnikov and J. Mesot, *Phys. Rev. B*, 2006, **73**, 094203.

42 C. Frontera, A. Caneiro, A. E. Carrillo, J. Oro-Sole and J. L. Garcia-Munoz, *Chem. Mater.*, 2005, **17**, 5439–5445.